

Temperature-insensitive tunable and stable Fabry-Perot cavity for atomic physics

Joshua Ruelle^{1,*}, Martin Hauden¹, Francisco S. Ponciano-Ojeda¹, and Marion Delehaye¹

¹Université Marie et Louis Pasteur, SUPMICROTECH, CNRS, Institut FEMTO-ST, F- 25000 Besançon, France

*corresponding author: joshua.ruelle@femto-st.fr

Abstract

Optical Fabry-Perot cavities are crucial tools for metrology experiments, where they achieve extreme length stability, and for some atomic physics experiments, where tunability to atomic transitions enables atom-light interactions. However, achieving both frequency stability and tunability in a single cavity has remained a challenge, forcing metrology experiments exploiting atom-cavity interactions to rely on external active feedback systems to stabilize the length of the cavity. Here, we describe a piezoelectrically-tunable cavity with a cancellation of the coefficient of thermal expansion at around 5°C, achieving fractional frequency instabilities at the 4×10^{-13} level for 1 s integration time. This advance eliminates the need for external stabilization in many atom-cavity experiments, making this design ideal for applications such as ultra-stable superradiant lasers and other cavity quantum electrodynamics experiments.

1 Introduction

Optical Fabry-Perot (FP) cavities are foundational to many cutting-edge systems in modern physics. Monolithic, ultra-stable FP cavities, achieving fractional frequency instabilities as low as $\sigma_y = 2.5 \times 10^{-17}$ [1, 2], are critical components of optical clocks, where they provide short-term frequency stability. Meanwhile, piezoelectrically-tunable cavities hosting cold atoms are used to mediate light-matter interactions in cavity quantum electrodynamics (cQED) systems. Recently, FP cavities have found a novel and challenging application at the intersection of time and frequency metrology and cQED: as the backbone of superradiant (SR) lasers operating as active optical clocks [3, 4], with the potential of achieving frequency instabilities as low as $4 \times 10^{-18}(\tau/s)^{-1/2}$ [5]. In these systems, an ensemble of atoms is coupled to an optical cavity, which must be precisely tuned to the resonant frequency of a narrow atomic transition. The atomic ensemble collectively emits a narrow-linewidth laser signal, with the emitted frequency remaining relatively insensitive to cavity detunings, thereby reducing the impact of cavity-induced frequency fluctuations by typically a factor 10^5 [6, 7]. Consequently, an ideally-performing superradiant laser targeting a fractional frequency instability of 4×10^{-18} would only require its optical cavity to achieve a fractional frequency instability on the order of 10^{-13} . Nevertheless, the residual fractional frequency instability of the cavity must still meet demanding standards, exceeding those typically required for conventional cQED experiments. The cavity must also be tunable to maintain resonance with the atomic transition, which introduces further technical complexity. Achieving simultaneously frequency stability and tunability,

two properties that are typically difficult to reconcile in a single device, thus represents a unique challenge.

Beyond its application in SR lasers, tunable and stable cavities are also highly relevant for other precision experiments, such as cavity-enhanced spectroscopy [8], or gravitational-wave detection: large, stable and tunable FP cavities enable applications such as frequency-dependent squeezing in the LIGO-VIRGO collaboration [9, 10, 11], or space-borne detectors like the eLISA mission [12], for which tunable and stable cavities have already been investigated [13].

In this context, we present the design of a piezoelectrically-tunable and stable FP cavity developed for an ytterbium (Yb) SR laser experiment. This paper is organized as follows: we first describe the design of the cavity and its materials, then the metrological methods that we use to characterize its performances, and finally the achieved results, including optical, thermal, electrical properties as well as its stability that reaches the mid- 10^{-13} range.

2 Composite cavity design

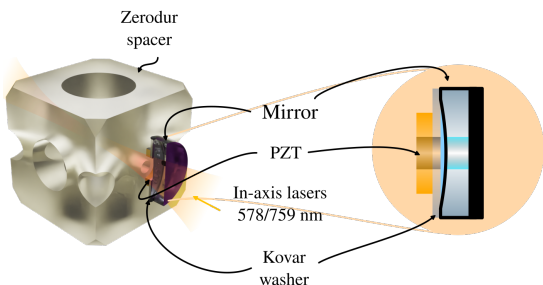


Figure 1: 3D representation of the tunable Fabry-Perot cavity consisting of a 50-mm long Zerodur spacer and mirrors stacked on a PZT ring and a Kovar washer.

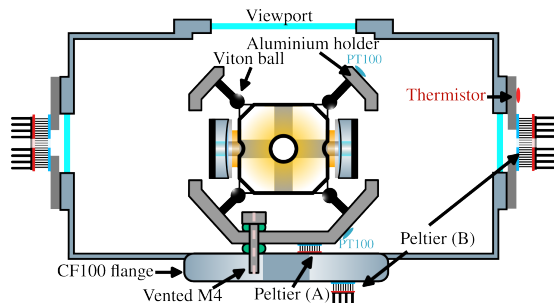


Figure 2: Schematic side-view of the cavity vacuum chamber.

For a superradiant laser, the cavity must satisfy four key criteria: **(i)** *optical access*, to enable the trap loading and imaging of atoms; **(ii)** *tunability*, to ensure resonance with the atomic transition; **(iii)** *frequency stability*, not to degrade the SR laser stability; and **(iv)** *high finesse* for suitable atom-cavity coupling.

To address these challenges, we developed a cavity design including a $L_{\text{ZD}} = 50$ mm-long cubic cavity spacer in Zerodur inspired by NPL design [14]. The spacer is mounted using a tetrahedral configuration, where four Viton balls are positioned at non-adjacent, diagonally opposed vertices of the cubic spacer. We modified the spacer to increase both the size and number of apertures **(i)**: the venting holes were enlarged to 20 and 28 mm, and 13-mm diameter holes have been added along the planar diagonal to allow for future improved atomic trapping (see Fig. 1). Using finite-element methods similar to those in [14], we optimized the depth of the corner cuts to 7.4 mm to minimize sensitivity to fluctuations of the holding forces. These simulations also estimate the acceleration sensitivity to less than $10^{-10} / (\text{m/s}^2)$ along all three axes.

Tunability **(ii)** is ensured using a pair of $L_{\text{PZT}} = 2$ mm-thick lead zirconate titanate (PZT) transducers. With a free stroke of $3.3 \mu\text{m}$ for a maximum voltage of 200 V, these PZTs allow the cavity to cover several free-spectral ranges.

Regarding frequency stability **(iii)**, the PZT actuators can degrade the stability by two different mechanisms. First, they convert electrical noise into mechanical length noise that directly translates into frequency instability. Thorough electrical filtering is therefore

essential. Second, they exhibit thermal expansion, characterized by a coefficient of thermal expansion $\alpha = \frac{1}{\Delta T} \frac{\Delta L}{L}$, where $\Delta L/L$ is the fractional length change induced by a temperature variation ΔT . The thermal expansion coefficient of the 2 mm-thick PZT actuators can be estimated between 0 °C and 50 °C [15] at around $\alpha_{\text{PZT}}(T) = a_{\text{PZT}}(T - T_{\text{PZT}})$, with $a_{\text{PZT}} = (-1.0 \pm 0.2) \times 10^{-7} \text{ K}^{-2}$ and $T_{\text{PZT}} = -0.9 \text{ °C}$, resulting in $\alpha_{\text{PZT}}(T = 25 \text{ °C}) = -2.6 \times 10^{-6} \text{ K}^{-1}$. Based on this estimation, we add between the PZT and the mirrors a pair of $L_{\text{Kov}} = 1$ mm-thick Kovar washers, which have a thermal expansion coefficient of $\alpha_{\text{Kov}} = 5.86 \times 10^{-6} \text{ K}^{-1}$ between 25 °C and 100 °C. The Zerodur spacer has a negligible thermal expansion coefficient $\alpha_{\text{ZD}} = 0 \pm 5 \times 10^{-8} \text{ K}^{-1}$ between 0 °C and 50 °C.

With these materials, the overall thermal noise floor is estimated at approximately 3×10^{-15} [16, 17], with roughly half of this contribution originating from the PZTs.

The cavity is designed to support a SR laser based on ytterbium atoms (**iv**). Consequently, the mirrors are highly-reflective at both the clock transition wavelength ($^1\text{S}_0 \leftrightarrow ^3\text{P}_0$) at 578 nm, and the so-called *magic wavelength* at 759 nm, where the light shifts of the $^1\text{S}_0$ and $^3\text{P}_0$ states are equal. The mirrors are identical, plano-concave with a 50 cm radius of curvature. The cavity is maintained under ultra-high vacuum conditions ($\leq 10^{-11}$ mbar).

3 Methods

To assess the performances of the cavity, we measure the frequency of a 578 nm laser¹, which is frequency-locked to the FP cavity using the Pound-Drever-Hall (PDH) technique [18, 19]. A 25 MHz EOM² is used to generate sidebands, and the reflected signal from the cavity is then detected, demodulated and fed to an ultra-fast PID³ to stabilize the laser frequency to the cavity resonance, achieving a lock bandwidth of roughly 600 kHz. The stabilized laser is then compared to an active hydrogen maser (H-maser) using an optical frequency comb⁴ to transfer fractional frequency stability from radio frequencies (RF) to the optical frequency domain. The OFC is locked on the H-maser with a fractional frequency instability $\sigma_y(\tau) = 10^{-13}(\tau/\text{s})^{-1/2}$ for all integration times τ between 1 and 10^5 s. The beatnote between the FP cavity-stabilized laser and the optical frequency comb is detected using a photodiode and mixed with an RF signal generated by a referenced Digital Direct Synthesizer (DDS) to produce a beatnote between 9.5 and 10.5 MHz for efficient filtering. This beatnote is finally acquired and analyzed using a frequency counter⁵.

4 Performances

4.1 Finesse measurement

To characterize the optical performances of the cavity, we employed the ring-down technique [20] to measure its finesse at 578 nm. Using a 105 ns fall-time photodiode, we initially measured a decay time of $(1.2 \pm 0.4) \mu\text{s}$ prior to the bake-out of the vacuum chamber, corresponding to a finesse of $21\,000 \pm 7000$. However, the mirror quality degraded during the bake-out process, resulting in a final decay time of $(411 \pm 2) \text{ ns}$ and a reduced finesse of 6920 ± 40 . Our hypothesis is a possible contamination from the Non-Evaporable Getter (NEG) pump that was activated during the bake-out.

¹Toptica DL-SHG Pro.

²Qubig PM7-VIS_25.

³Toptica FALC Pro.

⁴Toptica DFC.

⁵K+K Messtechnik.

4.2 Noise induced by PZT actuators

The cavity tunability is achieved using ring PZT actuators⁶ with a thickness of 2 mm and inner/outer diameters of 9 and 15 mm, respectively. We measured a piezoelectric cavity frequency sensitivity of 233 MHz/V. Such a high sensitivity allows the coverage of one free spectral range with an applied voltage of only 12 V but this induces also an increase of the absolute voltage noise influence on the cavity frequency.

The PZT actuators show mechanical resonances at approximately 110 kHz and 10 MHz, attributed to global mechanical transverse modes (due to misalignment of ceramic grains) and bulk transverse/longitudinal modes, respectively. The voltage noise of our most stable power supply⁷ was measured at $1 \mu\text{V}/\sqrt{\text{Hz}}$ at 1 Hz for 1 V output, which would result in a frequency noise of $0.2 \text{ kHz}/\sqrt{\text{Hz}}$ at 1 Hz. This noise level limits the fractional frequency stability of the cavity to approximately 5×10^{-13} [16]. Additionally, the residual voltage noise of $30 \text{ nV}/\sqrt{\text{Hz}}$ at 110 kHz excited the mechanical resonances of the PZT, which were visible in the beatnote spectrum. We therefore designed a DC low-pass filter ($R = 100 \text{ M}\Omega$, $C = 10 \mu\text{F}$) with a cutoff frequency at $160 \mu\text{Hz}$, similar to the design in [13]. For applications requiring fast actuation, the filter is AC-bypassed using a secondary filter ($R = 1.2 \text{ k}\Omega$, $C = 88 \text{ nF}$) providing a 1.6 kHz cutoff frequency for this branch. With the DC filter, the voltage noise has been reduced to $200 \text{ nV}/\sqrt{\text{Hz}}$, corresponding to a flicker contribution of 1×10^{-13} to the cavity fractional frequency instability.

4.3 Temperature control

The temperature stability of the cavity is achieved through a combination of active temperature regulation and passive thermal low-pass filtering. More specifically, the cavity is tetrahedrally-mounted via Viton balls within an aluminium holder under vacuum, which is attached to a CF100 flange (see Fig. 2). The aluminium holder is actively temperature regulated using two Peltier cells (Peltier (A) in Figure 2) which dissipate heat through the CF100 flange. The temperature is monitored in-loop and out-of-loop via PT100 thermistors, with regulation provided by a temperature controller⁸, ensuring a $0.1 \text{ K}(\tau/\text{s})^{-1/2}$ in-loop temperature stability. Passive thermal filtering is achieved by thermal isolation through the aluminium holder and Viton balls. An equivalent circuit model of the heat transfer from the vacuum chamber to the cavity, accounting for material properties and thermal radiation, showed a low-pass filter behavior with a $5.4 \mu\text{Hz}$ cut-off frequency. This is in agreement with the $\simeq 8 \text{ h}$ response time observed experimentally. To further reduce the system sensitivity to the lab temperature, the vacuum chamber is temperature regulated using several Peltier cells (Peltiers (B) in Figure 2). This secondary regulation reduced the out-of-loop residual temperature fluctuations by a factor 2. Remaining fluctuations are characterized by the Allan deviation of the out-of-loop temperature, below $2 \times 10^{-3} \text{ K}$ for all integration times.

4.4 Coefficient of thermal expansion

In order to explore the cavity frequency dependence on the temperature, we define a global coefficient of thermal expansion for the composite cavity as:

$$\alpha_{\text{tot}}(T) = \alpha_{\text{ZD}}(T) \frac{L_{\text{ZD}}}{L_{\text{tot}}} + \alpha_{\text{PZT}}(T) \frac{2L_{\text{PZT}}}{L_{\text{tot}}} + \alpha_{\text{Kov}}(T) \frac{2L_{\text{Kov}}}{L_{\text{tot}}}. \quad (1)$$

⁶Noliac NAC2124.

⁷Aim TTI EL155R.

⁸Wavelength electronics TC5-lab.

To our knowledge, the temperature dependence of the coefficients of thermal expansion α_{ZD} and α_{Kov} is not well-documented in the literature. In particular, for Kovar, only a global value for the broad temperature range between 25 °C and 100 °C is given ($\alpha_{\text{Kov}} = 5.86 \times 10^{-6} \text{ K}^{-1}$). To estimate $\alpha_{\text{tot}}(T)$, we performed the following experiment: starting from a thermally-stabilized system, we abruptly change the temperature set-point by 1 to 5 K. If $\alpha_{\text{tot}}(T)$ is nearly constant over the explored temperature range, the frequency response of the system is primarily an exponential with a time constant of approximately eight hours, corresponding to the global response time. However, if $\alpha_{\text{tot}}(T)$ changes sign over the temperature range, the frequency response exhibits non-monotonous behavior, with a turning point when the value of $\alpha_{\text{tot}}(T)$ vanishes.

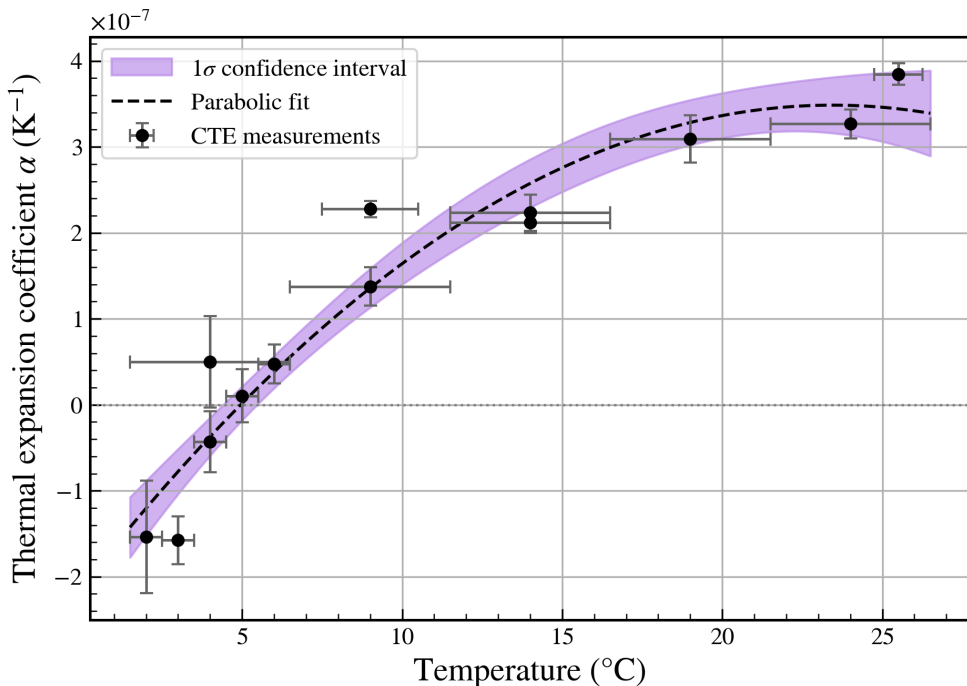


Figure 3: Cavity coefficient of thermal expansion measured by applying temperature steps to the cavity temperature set-point and measuring the subsequent changes in the 578 nm laser frequency. A zero-crossing point is extracted at $(4.9 \pm 0.5) \text{ }^\circ\text{C}$. Error bars are discussed in the main text.

Given potential temperature inhomogeneities during transient thermalization, we focused on the steady-state behavior. We measured the total frequency shift induced by temperature changes for various temperatures, as shown in Fig. 3. The horizontal error bars correspond to the temperature range explored during the step while the vertical error bars are obtained by taking the standard deviation of the fit residuals when fitting exponential-decay-like curves to traces. A cancellation of the thermal expansion coefficient is clearly visible, and a parabolic fit yielded a zero-crossing temperature $T_0 = (4.9 \pm 0.5) \text{ }^\circ\text{C}$. Near T_0 the temperature dependence of $\alpha_{\text{tot}}(T)$ can be approximated as $\alpha_{\text{tot}}(T) = a_{\text{tot}}(T - T_0)$ with $a_{\text{tot}} = (4.8 \pm 0.9) \times 10^{-8} \text{ K}^{-2}$. For the following best measurements, the regulation temperature was set to T_0 to minimize thermal expansion effects.

4.5 Stabilities

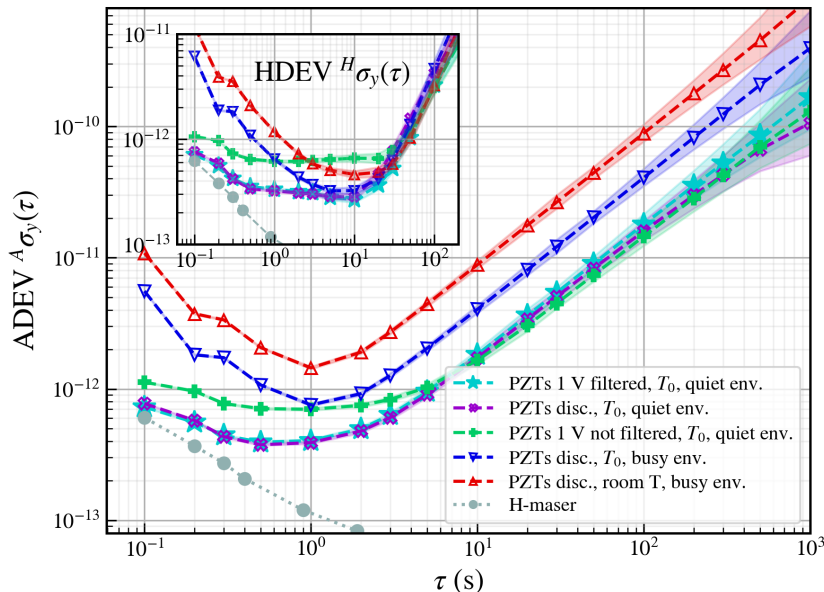


Figure 4: Fractional frequency stability of the tunable cavity measured against the H-maser, estimated using the unbiased Allan deviation under several conditions. Quiet environment (*ie* atomic oven off): regulated at T_0 with PZTs disconnected (pink stars), regulated at T_0 with filtered PZTs (purple squares), and regulated at T_0 with non-filtered PZTs at 1 V (green diamonds). Real operating conditions (atomic oven on): with PZTs disconnected at T_0 (blue lower triangles) and at room temperature (red upper triangles). Grey curve: fractional frequency stability of the H-maser measured against an ultra-stable cavity. Inset: unbiased Hadamard deviation of the same datasets, indicating the flicker frequency noise floor that could be achieved by suppressing frequency drift.

The fractional frequency stability of the cavity was estimated using the Allan deviation of the beatnote frequency between the FP cavity and the OFC referenced to the H-maser, and is shown in Fig. 4. The stability of the H-maser measured against an ultra-stable cavity at the 10^{-15} level is indicated as the grey curve in Fig. 4. We performed different measurement sets to properly characterize the contribution of the PZT noise on the overall stability. The best stability at one second was measured at 4×10^{-13} under two conditions: (1) when the PZTs were completely disconnected, or (2) when they were filtered with our custom lowpass filter. Both measurements were performed at the CTE zero-crossing temperature T_0 . This shows that the cavity stability is not limited by the PZT noise when filtered. Furthermore, additional measurements show a degradation of the stability of a factor ~ 2 when the PZTs are not filtered. Finally, real conditions measurements were done where the atomic oven is on and causes large temperature gradients around the chamber. The cavity stability remained in the 10^{-13} range at one second of integration time when operated at the T_0 temperature, while operation at room temperature with the oven showed a further degradation of the cavity stability by a factor 2.

To isolate the effects of linear drifts from other noise sources, we also analyzed the frequency data with Hadamard deviation (HDEV) in the inset of Fig. 4. The HDEV is by construction insensitive to linear drifts, and therefore mainly suppresses the effects of temperature fluctuations. For pure flicker frequency noise, this results in a τ^0 slope

in ADEV and HDEV, for which it can be shown that ${}^H\sigma_y(\tau) = \sqrt{\frac{8\ln 2 - 3\ln 3}{6\ln 2}} A \sigma_y(\tau) = 0.74^A \sigma_y(\tau)$ [21]. The HDEV plot emphasizes the degradation of the frequency stability induced by unfiltered power supplies, with a strong degradation of the flicker frequency noise. The short-term measurements (for $\tau = 100$ ms) are likely limited by the H-maser performances.

Overall, a fractional frequency stability of 8×10^{-13} at one second integration time is achievable for this free-running cavity under voltage-controlled conditions, and a realistic experimental environment that corresponds to the operational regime of a superradiant laser. This level of stability is sufficiently low to avoid limiting the performance of a SR laser above 8×10^{-18} at one second - a level of stability that has not been achieved by any system to date, with possible improvements down to 4×10^{-18} if the influence of the atomic oven can be reduced.

5 Conclusion

We have realized a tunable optical FP cavity that is passively stable at the 4×10^{-13} level in typical operating conditions. This cavity encompasses several optical accesses in order to couple atoms to its optical mode. This level of stability have been achieved thanks to the operation at the inversion temperature of the composite cavity at $(4.9 \pm 0.5)^\circ\text{C}$.

A better suppression of temperature-induced drifts could further improve the frequency stability of the system. This could be implemented by applying feed-forward or traditional PID methods [15, 22, 23] on the PZT voltage based on the lab temperature variations.

While this cavity has been designed with the purpose of the realization of an ytterbium superradiant laser, it can be used for other cQED experiments, or for applications requiring tunability and stability, such as gravitational wave interferometry.

Acknowledgements

The authors would like to thank Pierre Roset and Jacques Millo for providing the ultra-stable optical frequency reference, as well as Yann Kersalé for careful reading of the manuscript.

Funding information This work has been supported by the EIPHI Graduate school (contract ANR-17-EURE-0002) and by the Bourgogne-Franche-Comté Region, by the ANR (project CONSULA, ANR-21-CE47- 0006-02), by First-TF Labex (contract ANR-10-LABX-48-01), by Oscillator-IMP Equipex (contract ANR-11-EQPX-0033) and by the French Space Agency (CNES).

References

- [1] D. Lee, Z. Z. Hu, B. Lewis, A. Aeppli, K. Kim, Z. Yao, T. Legero, D. Nicolodi, F. Riehle, U. Sterr and J. Ye, *Frequency stability of 2.5×10^{-17} in a Si cavity with AlGaAs crystalline mirrors*, Phys. Rev. Lett. **136**(3), 033801 (2026), doi:10.1103/zgrm-cjbb.
- [2] D. G. Matei, T. Legero, S. Häfner, C. Grebing, R. Weyrich, W. Zhang, L. Sonderhouse, J. M. Robinson, J. Ye, F. Riehle and U. Sterr, *1.5 μm lasers with sub 10 mHz linewidth*, Phys. Rev. Lett. **118**(263202) (2017), doi:10.1103/PhysRevLett.118.263202.

- [3] D. Meiser, J. Ye, D. R. Carlson and M. J. Holland, *Prospects for a millihertz-linewidth laser*, Phys. Rev. Lett. **102**(163601) (2009), doi:10.1103/PhysRevLett.102.163601.
- [4] M. A. Norcia, J. R. K. Cline, J. A. Muniz, J. M. Robinson, R. B. Hutson, A. Goban, G. E. Marti, J. Ye and J. K. Thompson, *Frequency measurements of superradiance from the strontium clock transition*, Phys. Rev. X **8**(021036) (2018), doi:10.1103/PhysRevX.8.021036.
- [5] G. A. Kazakov, S. Dubey, A. Bychek, U. Sterr, M. Bober and M. Zawada, *Ultimate stability of active optical frequency standards*, Phys. Rev. A **106**(5), 053114 (2022), doi:10.1103/PhysRevA.106.053114.
- [6] S. J. M. Kuppens, M. P. van Exter and J. P. Woerdman, *Quantum-limited linewidth of a bad-cavity laser*, Phys. Rev. Lett. **72**(24), 3815 (1994), doi:10.1103/PhysRevLett.72.3815.
- [7] M. A. Norcia and J. K. Thompson, *Cold-strontium laser in the superradiant crossover regime*, Phys. Rev. X **6**(011025) (2016), doi:10.1103/PhysRevX.6.011025.
- [8] O. Axner, P. Ehlers, A. Foltynowicz, I. Silander and J. Wang, *NICE-OHMS—Frequency Modulation Cavity-Enhanced Spectroscopy—Principles and Performance*, pp. 211–251, Springer Berlin Heidelberg, ISBN 9783642400032, doi:10.1007/978-3-642-40003-2_6 (2014).
- [9] H. J. Kimble, Y. Levin, A. B. Matsko, K. S. Thorne and S. P. Vyatchanin, *Conversion of conventional gravitational-wave interferometers into quantum nondemolition interferometers by modifying their input and/or output optics*, Physical Review D **65**(2) (2001), doi:10.1103/physrevd.65.022002.
- [10] D. Ganapathy, W. Jia, M. Nakano, V. Xu, N. Aritomi, T. Cullen, N. Kijbunchoo, S. E. Dwyer, A. Mullavey, L. McCuller, R. Abbott, I. Abouelfettouh *et al.*, *Broadband quantum enhancement of the ligo detectors with frequency-dependent squeezing*, Physical Review X **13**(4) (2023), doi:10.1103/physrevx.13.041021.
- [11] F. Acernese, M. Agathos, A. Ain, S. Albanesi, C. Alléné, A. Allocca, A. Amato, C. Amra, M. Andia, T. Andrade, N. Andres, M. Andrés-Carcasona *et al.*, *Frequency-dependent squeezed vacuum source for the advanced virgo gravitational-wave detector*, Physical Review Letters **131**(4) (2023), doi:10.1103/physrevlett.131.041403.
- [12] K. Danzmann and A. Rüdiger, *LISA technology concept, status, prospects*, Classical and Quantum Gravity **20**(10), S1–S9 (2003), doi:10.1088/0264-9381/20/10/301.
- [13] K. Möhle, E. V. Kovalchuk, K. Döringshoff, M. Nagel and A. Peters, *Highly stable piezoelectrically tunable optical cavities*, Appl. Phys. B **111**(2), 223 (2013), doi:10.1007/s00340-012-5322-0.
- [14] S. Webster and P. Gill, *Force-insensitive optical cavity*, Optics Letters **36**(3572–3574) (2011), doi:10.1364/OL.36.003572.
- [15] C. Mangeot and B. Andersen, *Full characterisation of PZT actuators in quasi-static, large signal operation at elevated temperature*, Proc. Actuator 2016 (2016).
- [16] K. Numata, A. Kemery and J. Camp, *Thermal-noise limit in the frequency stabilization of lasers with rigid cavities*, Phys. Rev. Lett. **93**(25), 250602 (2004), doi:10.1103/PhysRevLett.93.250602.

- [17] T. Kessler, T. Legero and U. Sterr, *Thermal noise in optical cavities revisited*, Journal of the Optical Society of America B **29**(1), 178 (2012), doi:10.1364/JOSAB.29.000178.
- [18] R. W. P. Drever, J. L. Hall, F. V. Kowalski, J. Hough, G. M. Ford, A. J. Munley and H. Ward, *Laser phase and frequency stabilization using an optical resonator*, Applied Physics B Photophysics and Laser Chemistry **31**(2), 97 (1983), doi:10.1007/bf00702605.
- [19] E. D. Black, *An introduction to Pound–Drever–Hall laser frequency stabilization*, American Journal of Physics **69**(1), 79 (2001), doi:10.1119/1.1286663.
- [20] G. Rempe, R. Lalezari, R. J. Thompson and H. J. Kimble, *Measurement of ultralow losses in an optical interferometer*, Optics Letters **17**(5), 363 (1992), doi:10.1364/ol.17.000363.
- [21] E. Rubiola and F. Vernotte, *The companion of the Enrico’s chart for phase noise and two-sample variances*, doi:10.48550/arXiv.2201.07109 (2022).
- [22] D. Sabarianand, P. Karthikeyan and T. Muthuramalingam, *A review on control strategies for compensation of hysteresis and creep on piezoelectric actuators based micro systems*, Mechanical Systems and Signal Processing **140**, 106634 (2020), doi: 10.1016/j.ymssp.2020.106634.
- [23] H. Janocha and K. Kuhnen, *Real-time compensation of hysteresis and creep in piezoelectric actuators*, Sensors and Actuators A: Physical **79**(2), 83 (2000), doi: 10.1016/S0924-4247(99)00215-0.